Chapter 13

GHZ STATES WITH TIME-BIN QUBITS

This chapter includes the work published as:

[1] Samantha I. Davis, Chang Li, Rahaf Youssef, Neil Sinclair, Raju Valivarthi, and Maria Spiropulu. "Generation of Time-bin GHZ States." In: Optica Quantum 2.0 Conference and Exhibition. Optica Publishing Group, 2023, QTh4A.7. DOI: 10.1364/QUANTUM.2023.QTh4A.7. URL: https://opg.optica.org/abstract.cfm?URI=QUANTUM-2023-QTh4A.7.

13.1 Introduction

Quantum entanglement, one of the unique features of quantum mechanics, is a key ingredient for several quantum information processing fields including quantum communication, quantum computing, and quantum metrology. Maximally entangled bipartite states have not only been used for the above mentioned fields but were also crucial for fundamental tests of physics such as loophole-free tests of Bell inequalities [1, 2]. Analogous tripartite maximally entangled states have been proposed, known as Greenberger-Horne-Zeilinger (GHZ) states [3], which are shown to reject local realism theories without the need to acquire statistics on the measurements, and have known applications in distributed quantum computing [4] and multiparty quantum communication [5], such as superdense coding, quantum secret sharing, and quantum Byzantine agreements. Previous experimental proposals have been mostly limited to the polarization degree of freedom [6], until a recent experimental realization with energy-time entanglement [7]. Here we report our progress toward the first experimental demonstration of GHZ states with time-bin qubits[1], which are particularly well-suited for practical implementations in quantum networks for long-distance quantum communication and tests of nonlocality. Moreover, we develop a theoretical model to support the experimental results.

13.2 Entangling time-bin qubits with a switch

As described in Part I of this thesis, Bell pairs of time-bin qubits can be generated with high-fidelity using nonlinear optical processes such as SPDC. To generate

[1] At the time this work was conducted, we became aware of concurrent work published independently [8].

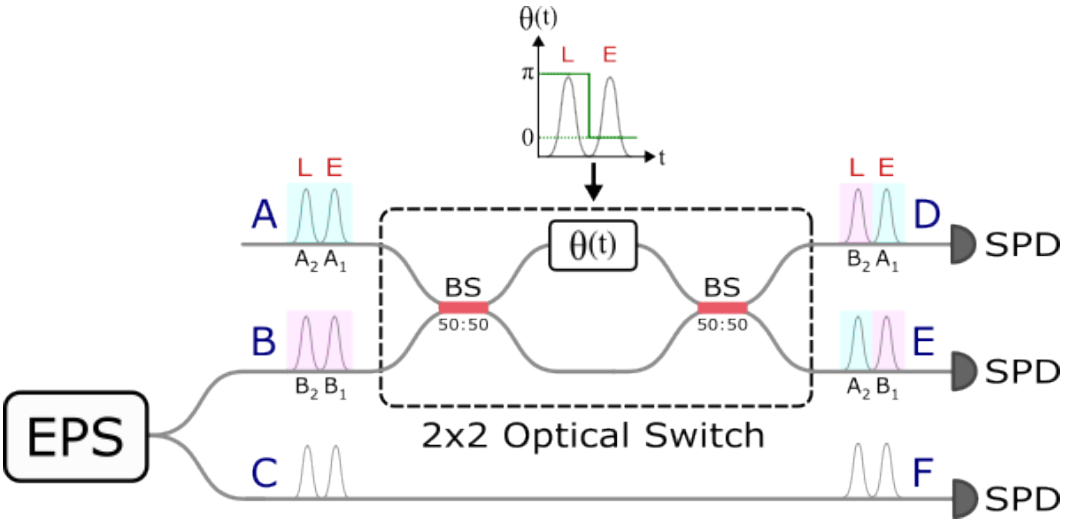

Figure 13.1: Setup for generating GHZ states with time-bin qubits. One member of a Bell pair produced by a entangled pair source (EPS) is interfered with another time-bin qubit using a 2x2 optical switch. A GHZ state is post-selected using single-photon detectors (SPDs) after the switch.

higher-order entangled states, we use the scheme proposed in Ref. [9] for entangling time-bin qubits. We generate a GHZ states by interfering one member of Bell pair with a third qubit in a 2-by-2 optical switch comprised of a balanced Mach-Zehnder interferometer (MZI) with a time-varying phase shift. The setup for the protocol is illustrated in Fig. 13.1.

Consider three qubits initialized in the state,

$$|\Psi\rangle = |\psi\rangle_A \otimes |\phi\rangle_{BC}\,, \tag{13.1}$$

$$|\psi\rangle_A = \frac{1}{\sqrt{2}}(|t_1\rangle_A + e^{i\phi_A}\,|t_2\rangle_A), \tag{13.2}$$

$$|\phi\rangle_{BC} = \frac{1}{\sqrt{2}}(|t_1\rangle_B\,|t_1\rangle_C + e^{i\phi_{BC}}\,|t_2\rangle_B\,|t_2\rangle_C), \tag{13.3}$$

where t_1 and t_2 denote the early and late time bins, respectively, and the subscripts on the states denote the spatial modes. Qubits at spatial modes A and B are inserted into the input ports the switch. The transformations of $|t_k\rangle_A$ and $|t_k\rangle_B$ through the switch are described by,

$$\begin{aligned} |t_k\rangle_A &\rightarrow \cos\left(\frac{\theta\,(t_k)}{2}\right)|t_k\rangle_D - \sin\left(\frac{\theta\,(t_k)}{2}\right)|t_k\rangle_E\,, \\ |t_k\rangle_B &\rightarrow \sin\left(\frac{\theta\,(t_k)}{2}\right)|t_k\rangle_D + \cos\left(\frac{\theta\,(t_k)}{2}\right)|t_k\rangle_E\,, \end{aligned} \tag{13.4}$$

where $k = 1, 2$ and $\theta(t_k)$ is the phase difference between the two arms of the MZI at time t_k. By setting $\theta(t_1) = 0$ and $\theta(t_2) = \pi$, the spatial modes of the input photons are unchanged in the early time bin and exchanged in the late time bin. The state of the system after the switch is,

$$|\psi\rangle_A \otimes |\phi\rangle_{\mathrm{BC}} \rightarrow \frac{1}{2}(|t_1\rangle_D |t_1\rangle_E |t_1\rangle_F + e^{i\phi_{BC}} |t_1\rangle_D |t_2\rangle_D |t_2\rangle_F \tag{13.5}$$

$$- e^{i\phi_A} |t_2\rangle_E |t_1\rangle_E |t_1\rangle_F - e^{i(\phi_A+\phi_{BC})} |t_2\rangle_D |t_2\rangle_E |t_2\rangle_F). \tag{13.6}$$

By measuring the three-fold coincidences at distinct spatial modes (D, E, F), we can post-select the time-bin GHZ state,

$$|\Psi_{GHZ}\rangle = \frac{1}{\sqrt{2}}(|t_1\rangle_D |t_1\rangle_E |t_1\rangle_F + e^{i\phi} |t_2\rangle_D |t_2\rangle_E |t_2\rangle_F). \tag{13.7}$$

13.3 Experiment

The experimental setup for generating time-bin GHZ states is shown in Fig. 13.2a. Time-bin qubits separated by 346 ps are created by injecting 1536 nm wavelength light from a continuous-wave laser into an intensity modulator (IM). The light is split into two paths by a 50:50 beamsplitter. In one path, the pulses are sent to a second harmonic generation (SHG) module containing an erbium doped fiber amplifer (EDFA) and PPLN waveguide, which up-converts the pulses to 768 nm. These pulses are used as a pump for type-II SPDC to create entangled photon pairs at 1536 nm. In the second path, the third qubit is prepared by attenuating the laser pulses. One member of the entangled state is interfered with the third qubit in a optical switch with a 20 GHz phase modulation bandwidth. Given two indistinguishable photons incident to the switch, the joint state of the three photons is described by a GHZ state after post-selection of the photons exiting the two output ports of the switch. The final output state is analyzed via measurements of the three photons (qubits) with superconducting nanowire single-photon detectors (SNSPDs) using a custom graphical user interface (see Fig. 13.2b).

13.4 Theory

We develop a theoretical model using the characteristic function-based formalism detailed in Chapter 9. The early and late time bins are modeled as independent modes, and the switch is modeled as a Mach-Zehnder interferometer with $\theta_E = 0$ for the early mode and $\theta_L = \pi$ for the late mode. Since the two-mode squeezed vacuum state and coherent state have Gaussian characteristic functions, and all subsequent operations up to detection are Gaussian, we construct the Symplectic matrix that

a)

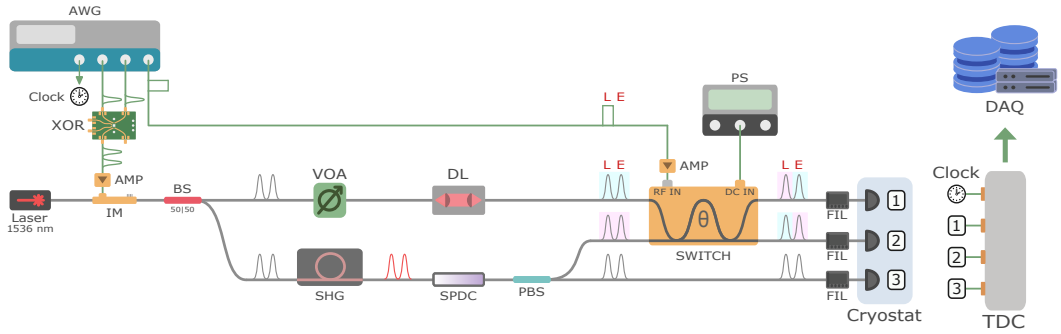

b)

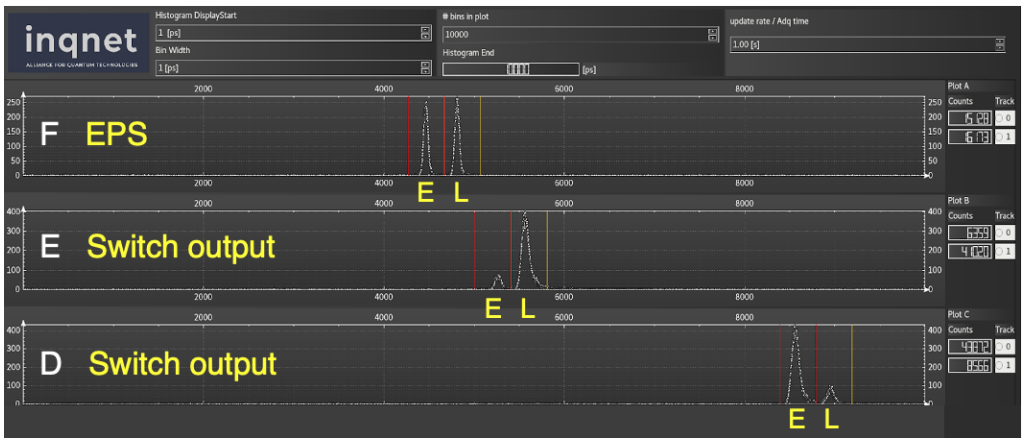

Figure 13.2: Experimental generation of time-bin GHZ states. a) Experimental setup. AWG, Tektronix AWG7002A; BS, Thorlabs 1550-nm fiber optic 50:50 beam splitter; DL, fiber optic delay line, EDFA, Pritel erbium-doped fiber amplifier; FIL, bandpass filter; Laser, MOGlabs Tunable Cateye Laser; PBS, Thorlabs 1550-nm fiber optic polarizing beam splitter; PPLN, HC Photonics waveguide; PS, power supply, SHG, Pritel optical fiber amplifier and second-harmonic generator; SNSPD, superconducting nanowire single-photon detector; TDC, quTAG time-to-digital converter; VOA, EXFO variable optical attenuator. b) Screenshot of custom Graphical User Interface (GUI) used for data acquisition and analysis. In the switch output channels, the larger peak corresponds to the weak coherent state and the smaller peak corresponds to one member of the TMSV state from SPDC. The discrepancy in peak heights is due to the different photon statistics and mean photon numbers of the coherent and TMSV states.

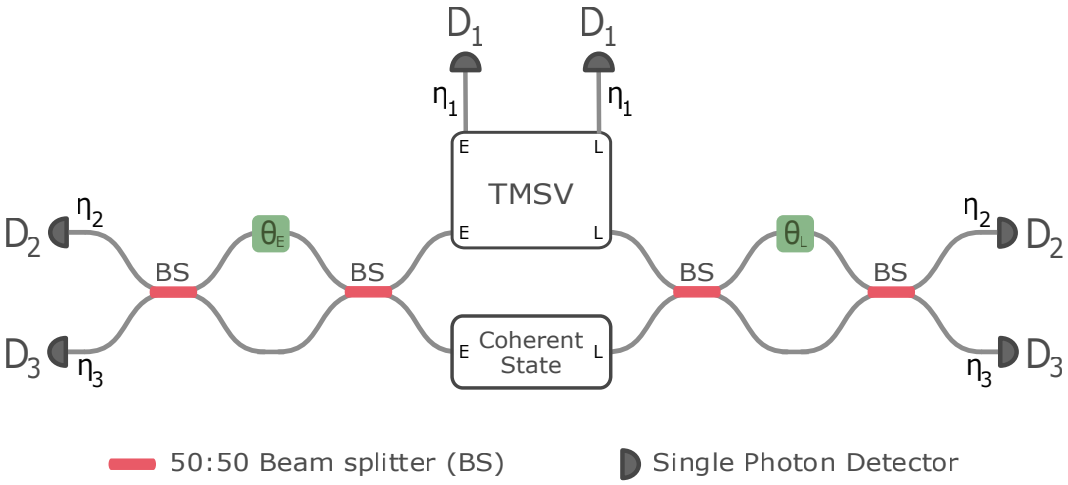

Figure 13.3: Setup for theoretical modeling. The top and bottom boxes represent a two-mode squeezed vacuum state (TMSV) and coherent state, respectively, in the product state of early and late temporal modes. Early and late temporal modes are represented as different spatial modes in the setup. The switch is modeled as an MZI acting on the early (late) modes of the coherent state and one half TMSV with phase shift $\theta_{E(L)}$. Measurement loss is modeled as mixing with a virtual vacuum mode with a beamsplitter (not depicted) with transmittances η_1, η_2, and η_3 for detectors D_1, D_2, and D_3, respectively.

maps the characteristic function of input state to that of the output state. The output characteristic function is found by substituting the displacement vector $\vec{d}$ and covariance matrix γ with $\vec{d} \rightarrow S^T\vec{d}$ and $\gamma \rightarrow S^T\gamma S$. From the output displacement vector and covariance matrix, the density matrix states produced in the experiment can be calculated as a function of relevant experimental parameters, such as the mean photon number of the coherent state μ_C, the mean photon number of the TMSV state (μ_s), measurement loss, and the extinction ratio of the switch. The extinction ratio of the switch is measured by setting the phase to $\theta = 0$ or π, sending strong coherent light into one input of the switch, and calculating the ratio of the powers measured from the output ports (P_D/P_E). Ideally, light is measured only in one output port or the other (P_D or $P_E = 0$). We measure extinction ratios of $|10\log_{10}(P_D/P_E)| \sim 18$ dB. Switch extinction ratios are modeled as $P_D/P_E = \cot^2(\theta_{E(L)}/2)$, where the phases $\theta_E \sim 0$ and $\theta_L \sim \pi$ are set to match the experimental extinction ratios.

From the output covariance matrix γ' and displacement vector $\vec{d}'$, we obtain a model for the density matrix of the experimental output state as a function of the mean photon numbers, losses and extinction ratio. The Fock basis density matrix

elements for an ℓ-mode Gaussian state ρ are in terms of its covariance matrix γ and displacement vector $\vec{d}$ are,

$$\langle \vec{m}| \rho |\vec{n}\rangle = T \times \text{lhaf}(\text{vid}(\mathbf{A}, \vec{\beta})), \tag{13.8}$$

$$T = \frac{\exp\left(-\frac{1}{2}\vec{d}^T \gamma^{-1} \vec{d}\right)}{\sqrt{\det(\gamma) \prod_{s=1}^{\ell} n_s! m_s!}}, \tag{13.9}$$

$$\mathbf{A} = \boldsymbol{X}\left(\mathbf{I}_{2\ell} - \gamma^{-1}\right), \quad \mathbf{X} = \begin{bmatrix} 0 & \mathbf{I}_\ell \\ \mathbf{I}_\ell & 0 \end{bmatrix}, \quad \vec{\beta}^T = \vec{d}^T \gamma^{-1}, \tag{13.10}$$

where $|\vec{n}\rangle = |n_1\rangle \cdots |n_\ell\rangle$ is the ℓ-mode photon number state of n_1 photons in the first mode, n_2 photons in the second mode, etc., $\text{lhaf}(\cdots)$ is the loop Hafnian, and $\text{vid}(\mathbf{A}, \vec{\beta}) = \mathbf{A} - \text{diag}(\text{diag}(\mathbf{A})) + \text{diag}(\vec{\beta})$ [10].

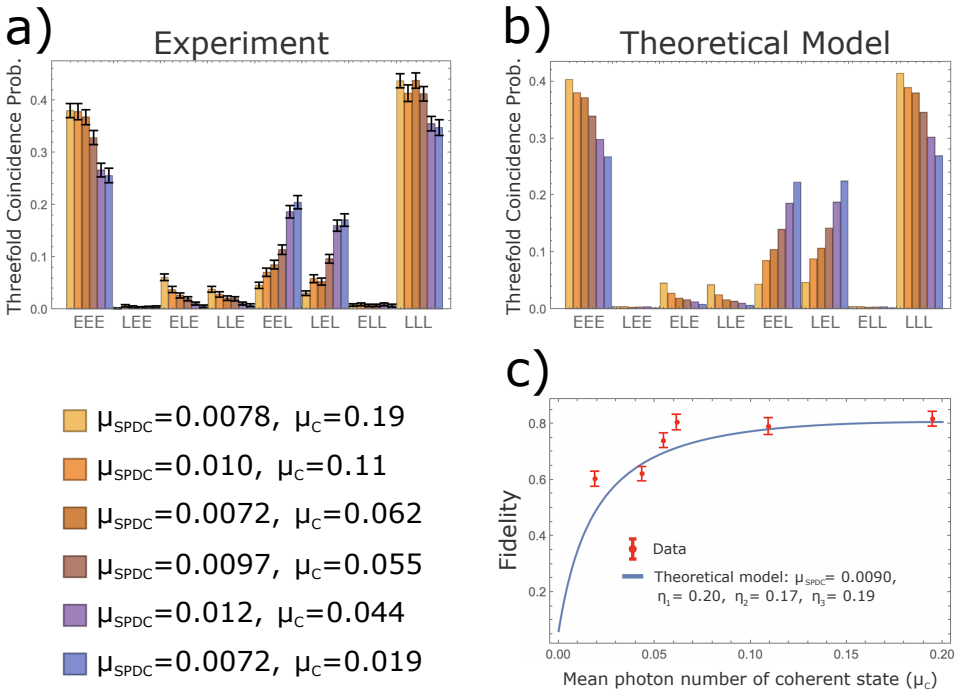

Figure 13.4: Characterization of time-bin GHZ states in the Z-basis. a) Threefold coincidence probabilities for varied mean photon number of the coherent state. The probabilities are found from dividing the coincidence rates in Hz by the repetition rate of the experiment (100 MHz). b) Theoretical model for the data in a). c) Z-basis fidelity for varied mean photon number of the coherent state. The error bars in a) and c) are calculated from Poisson statistics.

13.5 Results

With the measurement configuration in Fig. 13.2, we are able to perform projective measurements in the Z basis described by the measurement operators,

$$\hat{\Pi}_{i,j,k} = |t_i\rangle\langle t_i| \otimes |t_j\rangle\langle t_j| \otimes |t_k\rangle\langle t_k|, \tag{13.11}$$

where $i, j, k \in [1, 2]$. We measure the threefold coincidence rates,

$$C_{i,j,k} \propto \mathrm{Tr}[\hat{\rho}_{\mathrm{exp}}\hat{\Pi}_{i,j,k}],$$

for varied mean photon number of the coherent light (μ_C). The experimental and theoretical coincidence probabilities for each of the eight possible outcomes are shown in Fig. 13.4a and b, respectively. The coincidence probabilities are obtained by dividing the coincidence rates by the 100 MHz repetition rate of the experiment. The theoretical coincidence probabilities are calculated from the model using,

$$\mathrm{Tr}[\hat{\rho}\hat{\Pi}] = \left(\frac{1}{2\pi}\right)^N \int dx^{2N} \chi_\rho(x)\chi_\Pi(-x), \tag{13.12}$$

where N is the number of modes, $\chi(x)$ is the characteristic function of the output state and $\chi_\Pi(-x)$ is the characteristic function of the measurement operator of the detectors [11]. We define a "Z-basis fidelity" for the GHZ state as,

$$F_Z = \frac{P(t_1, t_1, t_1) + P(t_2, t_2, t_2)}{\sum_{i,j,k} P(t_i, t_j, t_k)}. \tag{13.13}$$

The Z-basis fidelity is plotted as function of the μ_C in Fig. 13.4c for the data in Fig 13.4a. The blue curve is the model using the average μ_{SPDC} of 0.009. The fidelity increases with μ_C for fixed μ_{SPDC} due to the mismatch in photon statistics for the coherent state and TMSV. We observe a maximum $F_Z = 82.0 \pm 4.1\%$ for $\mu_C = 0.19$.

In order to fully reconstruct the experimental states, a complete tomographic set of measurements need to be performed. This requires using interferometers before detection to project onto the X and Y bases. To estimate the overall state fidelity produced by our setup, we calculate the density matrix for $\mu_C = 0.19$ using Eq. 13.8. The density matrix elements are plotted in Fig. 13.5 for the ideal GHZ state, ρ_{GHZ}, and the model, ρ_{est}. The state fidelity is calculated as,

$$F(\rho_{\mathrm{est}}, \rho_{\mathrm{GHZ}}) = \left(\mathrm{Tr}\sqrt{\sqrt{\rho_{\mathrm{est}}}\rho_{\mathrm{GHZ}}\sqrt{\rho_{\mathrm{est}}}}\right)^2. \tag{13.14}$$

The model estimates a state fidelity of 80.6% for $\mu_C = 0.19$, $\mu_{\mathrm{TMSV}} = 0.009$, $\eta_1 = 0.2$, $\eta_2 = 0.17$, $\eta_3 = 0.19$, and an extinction ratio of 18 dB corresponding to $\theta_E = 0.25$, and $\theta_L = 0.25 + \pi$. By decreasing μ_{SPDC} to ~ 0.001, our model predicts $> 90\%$ fidelity can be achieved.

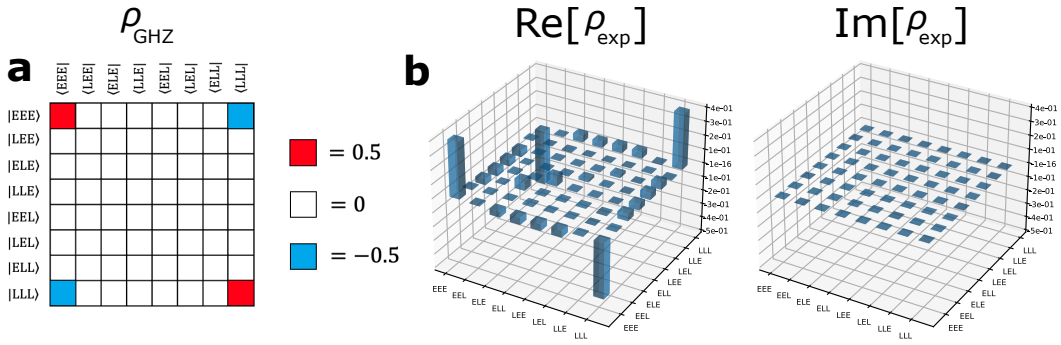

Figure 13.5: Density matrix model. a) Density matrix (ρ_{GHZ}) elements for an ideal GHZ state. b) Real and imaginary components of the density matrix model (ρ_{est}) for $\mu_C = 0.19$, $\mu_{\text{TMSV}} = 0.009$, $\eta_1 = 0.2$, $\eta_2 = 0.17$, $\eta_3 = 0.19$, and an extinction ratio of 18 dB corresponding to $\theta_E = 0.25$, and $\theta_L = 0.25 + \pi$.

References

[1] Marissa Giustina, Marijn AM Versteegh, Sören Wengerowsky, Johannes Handsteiner, Armin Hochrainer, Kevin Phelan, Fabian Steinlechner, Johannes Kofler, Jan-Åke Larsson, Carlos Abellán, et al. "Significant-loophole-free test of Bell's theorem with entangled photons." In: Physical Review Letters 115.25 (2015), p. 250401.

[2] Lynden K. Shalm, Evan Meyer-Scott, Bradley G. Christensen, Peter Bierhorst, Michael A. Wayne, Martin J. Stevens, Thomas Gerrits, Scott Glancy, Deny R. Hamel, Michael S. Allman, et al. "Strong loophole-free test of local realism." In: Physical Review Letters 115.25 (2015), p. 250402.

[3] Daniel M. Greenberger, Michael A. Horne, and Anton Zeilinger. "Going beyond Bell's theorem." In: Bell's theorem, quantum theory and conceptions of the universe. Springer, 1989, pp. 69–72.

[4] Ellie D'Hondt and Prakash Panangaden. "The computational power of the W and GHZ states." In: arXiv preprint quant-ph/0412177 (2004).

[5] Xing-Ri Jin, Xin Ji, Ying-Qiao Zhang, Shou Zhang, Suc-Kyoung Hong, Kyu-Hwang Yeon, and Chung-In Um. "Three-party quantum secure direct communication based on GHZ states." In: Physics Letters A 354.1-2 (2006), pp. 67–70.

[6] Anton Zeilinger, Michael A. Horne, Harald Weinfurter, and Marek Żukowski. "Three-particle entanglements from two entangled pairs." In: Physical Review Letters 78.16 (1997), p. 3031.

[7] Sascha Agne, Thomas Kauten, Jeongwan Jin, Evan Meyer-Scott, Jeff Z. Salvail, Deny R. Hamel, Kevin J. Resch, Gregor Weihs, and Thomas Jennewein. "Observation of Genuine Three-Photon Interference." In: Phys. Rev. Lett. 118 (15 Apr. 2017), p. 153602. DOI: 10.1103/PhysRevLett.118.153602. URL: https://link.aps.org/doi/10.1103/PhysRevLett.118.153602.

[8] Hsin-Pin Lo, Takuya Ikuta, Koji Azuma, Toshimori Honjo, William J Munro, and Hiroki Takesue. "Generation of a time–bin Greenberger–Horne–Zeilinger state with an optical switch." In: Quantum Science and Technology 8.3 (Apr. 2023), p. 035003. DOI: 10.1088/2058-9565/acc7c2. URL: https://dx.doi.org/10.1088/2058-9565/acc7c2.

[9] Hiroki Takesue. "Entangling time-bin qubits with a switch." In: Physical Review A 89.6 (2014), p. 062328.

[10] Nicolás Quesada, Luke G. Helt, Josh Izaac, Juan Miguel Arrazola, Reihaneh Shahrokhshahi, Casey R. Myers, and Krishna K. Sabapathy. "Simulating realistic non-Gaussian state preparation." In: Physical Review A 100.2 (2019), p. 022341.

[11] Masahiro Takeoka, Rui-Bo Jin, and Masahide Sasaki. "Full analysis of multi-photon pair effects in spontaneous parametric down conversion based photonic quantum information processing." In: New Journal of Physics 17.4 (2015), p. 043030.